Int. J. Electrochem. Sci., 13 **(2018)** 7655 – 7662, doi: 10.20964/2018.08.10

International Journal of ELECTROCHEMICAL SCIENCE
www.electrochemsci.org

Structural and electrochemical properties of nanolayer-stacking structured copper-doped nickel hydroxide

Kyung Ho Kim[*], *Moe Mikami, Yoshio Abe, Midori Kawamura, Takayuki Kiba*

Department of Materials Science and Engineering, Kitami Institute of Technology, 165 Koen-cho, Kitami, Hokkaido 090-8507, Japan
[*]E-mail: khkim@mail.kitmai-it.ac.jp

Received: 10 March 2018 / *Accepted:* 1 May 2018 / *Published:* 5 July 2018

Copper-doped nickel hydroxide (Cu:$Ni(OH)_2$) was synthesized via a facile wet-chemical method and its structural and electrochemical properties were compared to those of pure nickel hydroxide ($Ni(OH)_2$). After Cu incorporation, the morphology of the $Ni(OH)_2$ nanostructures could be easily tuned from a curved nanolayered structure to a nanolayer-stacking structure. Both samples were hydrophilic. Furthermore, even though no additional conductive and binder materials were employed, the Cu:$Ni(OH)_2$ sample exhibited better pseudocapacitance performance than the $Ni(OH)_2$ sample. These results confirmed that the Cu:$Ni(OH)_2$ sample, which can be prepared by an easy low-cost method, shows great potential for application in electrochemical devices.

Keywords: Nickel hydroxide, Copper, Nanolayer-stacking structure, Nanosheets

1. INTRODUCTION

Hierarchical nanostructures of nickel hydroxide ($Ni(OH)_2$) have been extensively investigated because of their potential application as materials in various electronic and optoelectronic applications [1-3]. Recently, the introduction of 1-dimensional (1D) carbon nanotubes (CNTs) and 2-dimensional (2D) reduced graphene oxide (rGO) into $Ni(OH)_2$ was demonstrated as an effective way to modify the morphology of $Ni(OH)_2$ nanostructures and improve their electrochemical performance. These nanostructures are usually prepared via a two-step approach [4-6]. However, the addition of a dopant to the precursor aqueous solution could provide a simple one-step wet-chemical method [7-12]. He et al. reported that the incorporation of Cu in the nickel oxide (NiO) structure is an easy way to improve the electrochromic behavior of the material [9]. In our previous study, we reported the effect of Cu incorporation on a nanocrystalline NiO thin film prepared by a sol-gel spin coating method [10]. With

the addition of a small amount of Cu, the Cu-doped NiO thin film exhibited decreased resistivity but increased crystalline size over those of the pure NiO thin film. Recently, Zheng et al. reported that ultrafine nickel-copper carbonate hydroxide ($NiCu(OH)_2CO_3$) nanowire network arrays on Cu foam exhibited excellent electrochemical performance [11]. Moreover, Shruthi et al. reported that the addition of CuO to $Ni(OH)_2$ enhanced the electrochemical response of the compound [12]

In this study, we prepared a 2D nanolayer-stacking structured Cu-doped nickel hydroxide ($Cu:Ni(OH)_2$) film via a simple one-step process and compared its structural and electrochemical properties to those of pure $Ni(OH)_2$.

2. EXPERIMENTAL

The $Ni(OH)_2$ sample comprised a simple aqueous solution of nickel acetate tetrahydrate ($Ni(CH_3COO)_2{\cdot}4H_2O$, Ni(Ac), 10 mM) and hexamethylenetetramine ($C_6H_{12}N_4$, HMT, 10 mM). Copper acetate monohydrate ($Cu(CH_3COO)_2{\cdot}H_2O$, Cu(Ac), 0.5 mM) was added as a dopant to the precursor aqueous solution to afford the $Cu:Ni(OH)_2$ sample. The reaction was performed at 95 ºC for 6 h; detailed fabrication processes have been reported in our previous study [13]. Finally, the as-prepared $Ni(OH)_2$ and $Cu:Ni(OH)_2$ nanostructures were dried at 90 ºC for 24 h in air.

The crystalline phase and morphology were examined by X-ray diffraction (XRD, D8 ADVANCE) and field emission scanning electron microscopy (FESEM, JSM-6701F), respectively. The composition was analyzed using an energy dispersive X-ray spectroscopy (EDS) attached to the FESEM. Chemical bonds were identified by Fourier transform infrared spectroscopy (FTIR, FT/IR-6100), while the water contact angle was measured using DropMaster DM100.

The electrochemical performance was evaluated by cyclic voltammetry (CV, HOKUTO DENKO, HZ-7000). The typical three-electrode system employed comprised of a 2 M KOH aqueous solution as the electrolyte, a Pt foil as the counter electrode, and a Ag/AgCl as the reference electrode. The active materials (~0.18 mg and 0.20 mg for $Ni(OH)_2$ and $Cu:Ni(OH)_2$, respectively) were drop-casted on poly(ethylenimine) (PEI)-coated indium tin oxide (ITO)/glass substrates and subsequently dried at 90 ºC for 24 h in air. The active materials did not require further annealing and no additional conductive or binder materials were employed.

3. RESULTS AND DISCUSSION

Figure 1 presents the XRD patterns of the $Ni(OH)_2$ (a) and $Cu:Ni(OH)_2$ (b) samples prepared on glass substrates. For the $Ni(OH)_2$ sample, diffraction peaks of 19.1º, 31.9º, and 38.4º, at the 2θ position, were indexed to the (001), (100), and (101) planes of hexagonal β-$Ni(OH)_2$ (JCPDS Card No. 14-0117), respectively. $Ni(OH)_2$ was formed from the reaction between the Ni^{2+} ions released from the Ni(Ac) precursor and the OH^- ions afforded from the decomposition of the HMT [14]. Additionally, weak diffraction peaks at the 2θ position of 9.5º and 14.5º were assigned, respectively, to the (002) and (110) planes of the base-centered monoclinic $NiCO_3{\cdot}6H_2O$ (JCPDS Card No. 12-0276). Following the

incorporation of Cu, diffraction peaks at the 2θ position of 10.7º and 21.7º were indexed, respectively, to the (003) and (006) planes of rhombohedral nickel hydroxide hydrate (α-$Ni(OH)_2 \cdot 0.75H_2O$) (JCPDS Card No. 38-0715). These results implied the formation of a layered structure. However, these diffraction peaks shifted toward a lower diffraction angle compared to those observed for standard α-$Ni(OH)_2$. This was attributed to the incorporation of Cu ions and/or intercalation with various anions [14]. In our previous study, a similar tendency was observed when the reaction temperature was varied [15]. Thus, after decreasing the reaction temperature to 70 ºC, a marked increase in the intensity of the diffraction peaks indexed as the α-$Ni(OH)_2$ phase was observed [15]. No diffraction peaks related to the copper carbonate hydroxide ($Cu_2(OH)_2CO_3$) and copper hydroxide ($Cu(OH)_2$) phases were observed, possibly because the Cu ions could be easily substituted for the Ni ions [10,16-18].

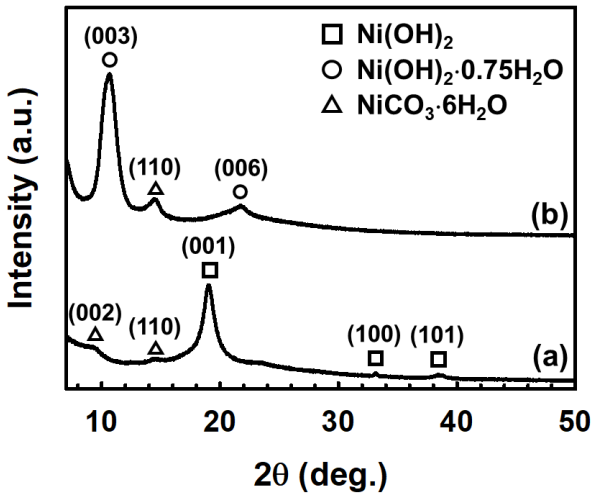

Figure 1. XRD patterns of $Ni(OH)_2$ (a) and $Cu:Ni(OH)_2$ (b) samples.

Figure 2 illustrates the FTIR spectra of $Ni(OH)_2$ (a) and $Cu:Ni(OH)_2$ (b) samples prepared on Si substrates. The two sharp strong peaks at 3640 cm^{-1} and 510 cm^{-1} in the $Ni(OH)_2$ sample were attributed to non-hydrogen bonded OH and Ni-OH bonds [19], respectively. These peaks provided ample evidence for the formation of well crystallized $Ni(OH)_2$. With the incorporation of Cu, the OH peaks still appeared but with decreased relative intensities. Moreover, the bonds around 3460 cm^{-1} and 1600 cm^{-1}, associated with the stretching and bending vibrations of the hydrogen bonded water [19], become stronger. The $Cu:Ni(OH)_2$ sample displayed strong absorption peaks around 650 cm^{-1}. This was ascribed to CO_3^{2-} bending vibration modes (marked by asterisk) [20] and indicated a diffraction peak shift. Both samples displayed absorption peaks related to C-H stretching (~2844 cm^{-1}), CO_3^{2-} stretching vibration (~1370 cm^{-1}), and C-N vibration (~1332 cm^{-1}, 1195 cm^{-1}, and 985 cm^{-1}) modes. The FTIR and XRD results were in good agreement with each other and revealed efficient formation of the nickel-based hydroxide phase.

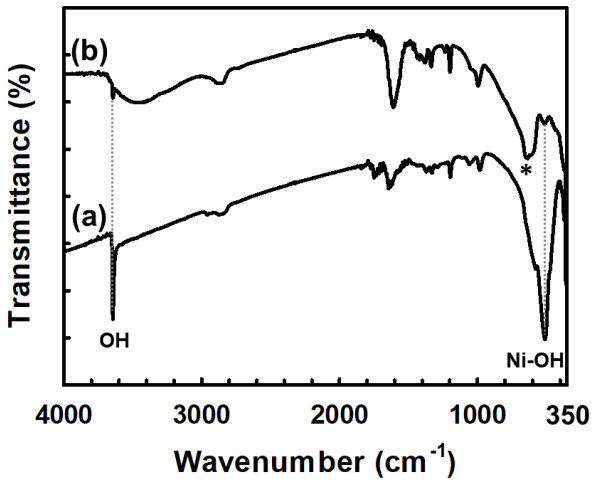

Figure 2. FTIR spectra of $Ni(OH)_2$ (a) and $Cu:Ni(OH)_2$ (b) samples.

Figure 3 displays FESEM images of the $Ni(OH)_2$ (a-c) and $Cu:Ni(OH)_2$ (d-f) samples prepared on Si substrates. The top (a) and cross-sectional (b,c) images reveal that the $Ni(OH)_2$ sample comprised interconnected 2D nanosheets [thickness ~20 nm; Fig.3(c)] that led to the formation of curved nanolayered structures. Detailed morphological evolution of the $Ni(OH)_2$ sample for various reaction times and annealing temperatures has been discussed in our previous paper [13,15]. With the addition of Cu, the sample displayed a unique morphology. Compared to the $Ni(OH)_2$ sample, the Cu:

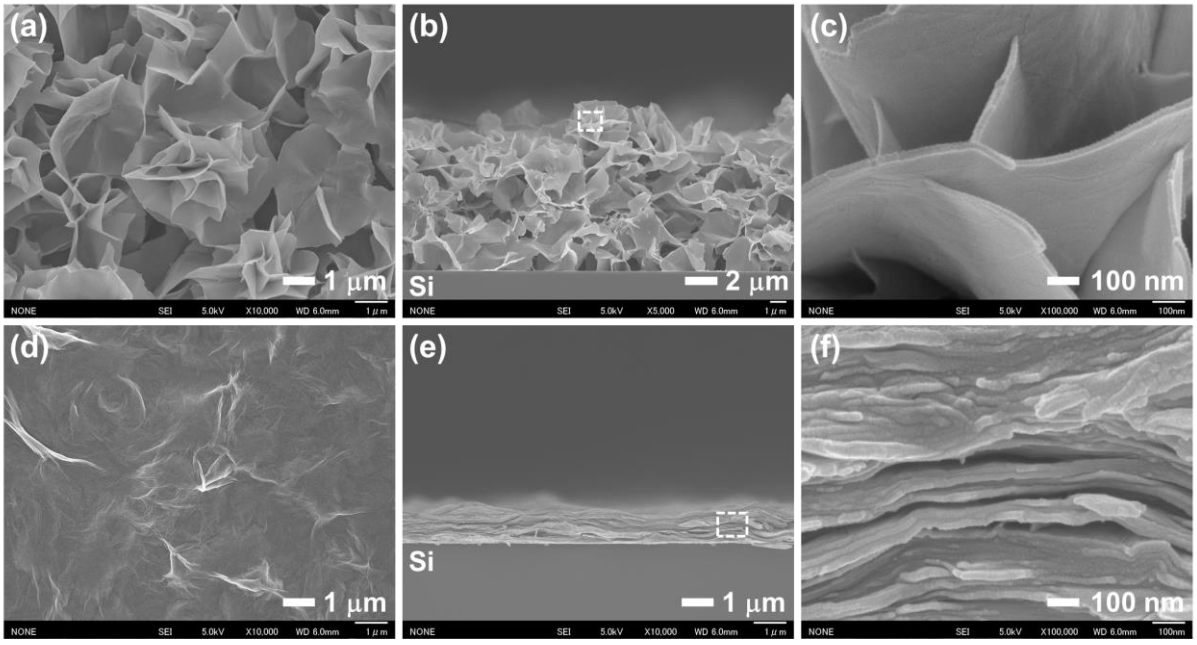

Figure 3. FESEM images of $Ni(OH)_2$ (a-c) and $Cu:Ni(OH)_2$ (d-f) samples; (c) and (f) are higher magnification images of the dotted squares in (b) and (e), respectively.

$Ni(OH)_2$ sample presented fewer protruding nanosheets (bright) and more flat area (grey) on its surface (Fig.3(d). The cross-sectional images (e,f) reveal that the $Cu:Ni(OH)_2$ sample exhibits a nanolayer-stacking structure (nanolayer thickness ~20 nm); this is in agreement with the XRD result (Fig.1(b)). With the incorporation of Cu, the nucleation rate for the formation of the nanosheets decreased, thereby leading to an increased flat area (grey) on the surface of the $Cu:Ni(OH)_2$ sample. Comparable results were observed for the morphological evolution of different reaction temperatures [15]. Similar layer-stacking structures have been reported for a layered MgAl-double hydroxide prepared by the electrophoretic deposition (EPD) [21]; however, the nanolayer-stacking morphology of the nickel-based hydroxide nanostructures is unique and critical to their overall functionality in the proposed application [22-24]. Both EDS spectrum and elementary mapping images revealed that Cu and Ni are spread uniformly over the entire surface (Fig.4.).

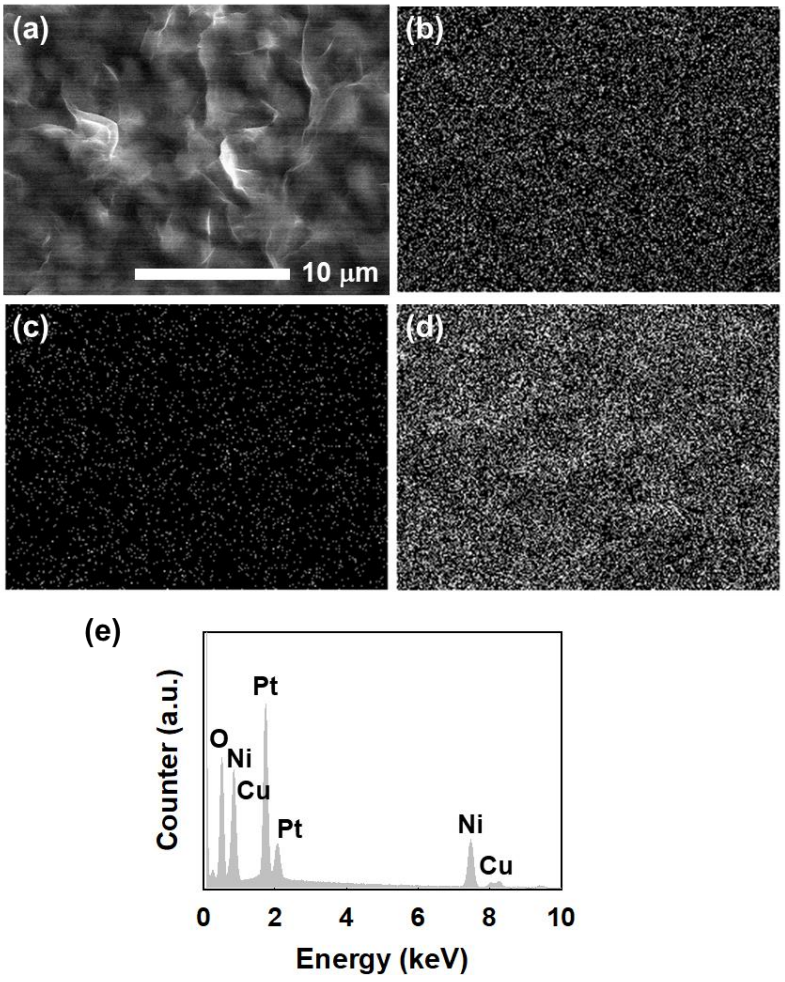

Figure 4. Electron image (a), EDS elemental mappings (b-d) and spectrum (e) of the $Cu:Ni(OH)_2$ sample; (b) Ni, (c) Cu, (d) O.

Water contact angles were measured to investigate the surface wettability of the two samples. The water contact angle of the $Cu:Ni(OH)_2$ sample was 37º, whereas water seeped into the surface of

the $Ni(OH)_2$ sample. These results suggest that both samples exhibit hydrophilicity, an essential property for their applications as electrochemical supercapacitors [25].

Figure 5(a) shows the CV curves of the $Ni(OH)_2$ and $Cu:Ni(OH)_2$ samples at a scan rate of 20 mV/s. The inset reveals that the $Ni(OH)_2$ sample exhibits poor electrochemical activity, while the CV curve of $Cu:Ni(OH)_2$ sample implies pseudocapacitive characteristics. In addition the $Cu:Ni(OH)_2$ sample presented better electrochemical activity than the $Ni(OH)_2$ sample. Two anodic peaks at 0.35 V and 0.39 V were attributed to the oxidation of β-$Ni(OH)_2$ to β-NiOOH and phase transformation of α-$Ni(OH)_2$ to β-$Ni(OH)_2$, respectively, while the cathodic peak at 0.28 V was attributed to the reverse process, namely β-NiOOH to β-$Ni(OH)_2$ [2]. Figure 5(b) depicts the CV curves of the $Cu:Ni(OH)_2$ sample for scan rate ranging from 5 to 100 mV/s. No distortion in the symmetry of the CV curves was observed with an increase in the scan rate. The current density clearly increased with increasing scan rate and all the CV curves maintained a similar shape indicating that the $Cu:Ni(OH)_2$ sample favored fast redox reactions. In addition, the large planar surface of the nanolayer-stacking structured $Cu:Ni(OH)_2$ can facilitate electron transfer from the $Cu:Ni(OH)_2$ to the ITO electrode. Figure 5(c) shows that both anodic (square) and cathodic (circle) peak current densities are linearly proportional to the square root of the scan rate, demonstrating the quasi-reversible behavior of the $Cu:Ni(OH)_2$ electrode [26]. The specific capacitance C (F/g) was calculated from the following equation [27]:

$$C = \frac{I}{2mvV}$$

where m and v are the mass and scan rate, respectively. V is the potential window, and I is the integrated area of the CV curve in one complete cycle. The calculated specific capacitance values of the $Cu:Ni(OH)_2$ sample are ~24, 17, 14, 10, and 8 F/g at scan rates of 5, 10, 20, 50, and 100 mV/s, respectively. These values were quite small compared to those (450 – 1667 F/g @ 5 mV/s) reported in other studies [2,3]. However, those samples were prepared on metal foam substrates mixed with conductive and/or binder materials and subsequently, pressure was applied to increase adhesion between the active materials and the substrates. On the contrary, in this study, the $Ni(OH)_2$ and $Cu:Ni(OH)_2$ nanostructures were working electrodes directly prepared on PEI coated ITO/glass substrates without using any additional carbon black conductive material and polytetrafluoroethylene (PTFE) binder material for the CV test. Moreover, the reaction and dry temperatures were significantly lower than those reported in literatures [1,28,29]. Figure 5(d) presents the CV curves of the $Cu:Ni(OH)_2$ sample at 20 mV/s with cycling. After 100 cycles, the initial specific capacitance deteriorated by ~15% [inset in Fig.5(d)]. This may be due to partial exfoliation of the $Cu:Ni(OH)_2$ sample from the ITO/glass substrate during cycling. However, no cracks were observed on the sample after cycling. Further adjustments of the adhesion between the $Cu:Ni(OH)_2$ sample and ITO/glass substrate are necessary to improve the electrochemical properties of the material.

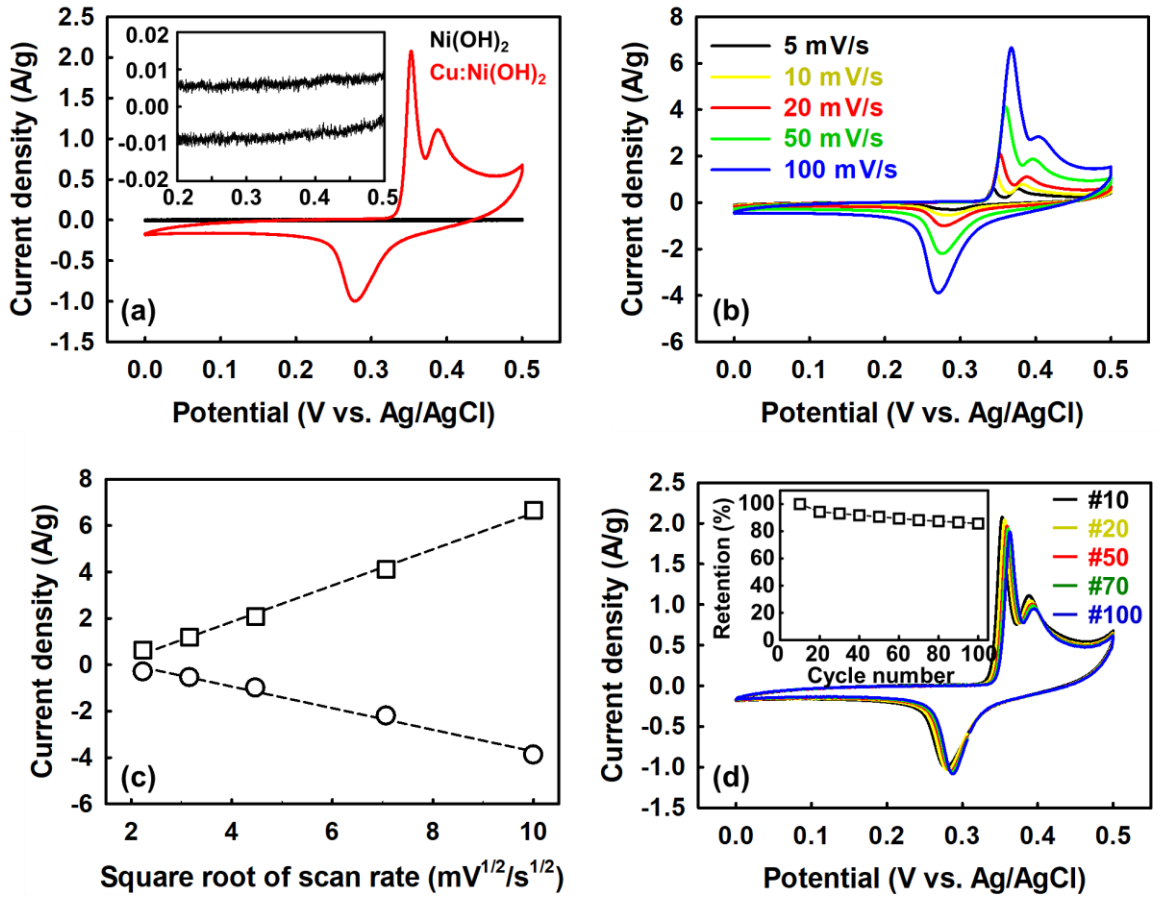

Figure 5. CV curves of $Ni(OH)_2$ and $Cu:Ni(OH)_2$ samples at a scanning rate of 20 mV/s (a), CV curves of the $Cu:Ni(OH)_2$ sample at various scanning rates (b), plot of anodic and cathodic current densities versus the square root of scan rates (c), and CV curves of the $Cu:Ni(OH)_2$ sample at the scan rate of 20 mV/s up to 100th cycle (d); inset in (a) is an enlarged view of the CV curve of the $Ni(OH)_2$ sample; inset in (d) is the retention of the specific capacitance.

4. CONCLUSIONS

We have successfully synthesized the polycrystalline phase of $Ni(OH)_2$ and $Cu:Ni(OH)_2$ via a simple one-step approach at a reaction temperature of 95 ºC. With the incorporation of Cu, the curved nanolayered structure was transformed into a nanolayer-stacking structure. Both the $Ni(OH)_2$ and $Cu:Ni(OH)_2$ samples exhibited a hydrophilic nature. Additionally, the $Cu:Ni(OH)_2$ sample exhibited a significantly improved electrochemical reaction activity over the $Ni(OH)_2$ sample. Therefore, we concluded that the $Cu:Ni(OH)_2$ nanostructure, prepared via a cost-effective one-step method, shows great potential for application in future supercapacitors.

ACKNOWLEDGEMENT
This work was supported by a Grant-in-Aid for Scientific Research (C) (No. 17K06336) from the Japan Society for the Promotion of Science.

References

1. Y. Wang and Q. Zhu, *Mater. Res. Bull.*, 45 (2010) 1844.
2. S.R. Ede, S. Anantharaj, K.T. Kumaran, S. Mishra, and S. Kundu, *RSC Adv.*, 7 (2017) 5898.
3. H.B. Li, M. H. Yu, F.X. Wang, P. Liu, Y. Liang, J. Xiao, C.X. Wang, Y.X. Tong, and G.W. Yang, *Nat. Commun*., 4 (2013) 1897.
4. Y. Liu, R. Wang, and X. Yan, *Sci. Rep*., 5 (2015)11095.
5. Eduardo G.C. Neiva, Márcela M. Oliveira, Marcio F. Bergamini, Luiz H. Marcolino Jr, and Aldo J.G. Zarbin, *Sci. Rep.*, 6 (2016) 33806.
6. R.R. Salunkhe, J. Lin, V. Malgras, S.X. Dou, J.H. Kim, and Y. Yamauchi, *Nano Energy*, 11 (2015) 211.
7. A. Vanaja, G.V. Ramaraju, and K. Srinvivasa Rao, *Indian Journal of Science and Technology*, 9 (2016) 1.
8. C-Y. Chiang, Y. Shin, and S. Ehrman, *J. Electrochem. Soc*., 159 (2012) B227.
9. Z. He, Z. Ji, S. Zhao, C. Wang, K. Liu, and Z. Ye, *Solar Energy*, 80 (2006) 226.
10. K.H. Kim, C. Takahashi, Y. Abe, and M. Kawamura, *Optik*, 125 (2014) 2899.
11. X. Zheng, Y. Ye, Q. Yang, B. Geng, and X. Zhang, *Chem. Eng., J*. 290 (2016) 353.
12. B. Shruthi, B.J. Madhu, V. Bheema Raju, S. Vynatheya, B.Veena Devi, G.V. Jayashree, and C.R. Ravikumar, *Journal of Science: Advanced Materials and Devices*, 2 (2017) 93.
13. K.H. Kim, M. Mikami, Y. Abe, M. Kawamura, and T. Kiba, *Thin Solid Films*, 654 (2018) 49.
14. B-H. Liu, S-H. Yu, S-F. Chen, and C-Y. Wu, *J. Phys. Chem*., B 110 (2006) 4039.
15. M. Mikami, K.H. Kim, Y. Abe, M. Kawamura, and T. Kiba, *Proceedings of IDW*, 24 (2017) 1397.
16. S.C. Chen, T.Y. Kuo, Y.C. Lin, and H.C. Lin, *Thin Solid Films*, 519 (2011) 4944.
17. X. Chen, L. Zhao, and Q. Niu, *J. Electron. Mater*., 41 (2012) 3382.
18. A. Liu, H. Zhu, Z. Guo, Y. Meng, G. Liu, E. Fortunato, R. Martins, and F. Shan, *Adv. Mater*., 17 (2017) 1599.
19. M. Pérez-Morales, E. Muñoz, M.T. Martín-Romero, and L. Camacho, *Langmuir*, 21 (2005) 5468.
20. G. Zhu, C. Xi, M. Shen, C. Bao, and J. Zhu, *ACS Appl. Mater. Interfaces*, 6 (2014) 17208.
21. A. Matsuda, H. Sakamoto, Mohd Arif Bin Mohd Nor, G. Kawamura, and H. Muto, *J. Phys. Chem*. B, 117 (2013) 1724.
22. J. Li, M. Yang, J. Wei, and Z. Zhou, *Nanoscale*, 4 (2012) 4498.
23. J.W. Lee, J.M. Ko, and J-D. Kim, *J. Phys. Chem*. C, 115 (2011) 19445.
24. G.S. Gund, D.P. Dubal, D.S. Dhawale, S.S. Shinde, and C.D. Lokhande, *RSC Adv*., 3 (2013) 24099.
25. D.P. Dubal, D.S. Dhawale, R.R. Salunkhe, V.S. Jamdade, and C.D. Lokhande, *J. Alloys Compd*., 492 (2010) 26.
26. B. Wang, Q. Liu, Z. Qian, X. Zhang, J. Wang, Z. Li, H. Yan, Z. Gao, F. Zhao, and L. Liu, *J. Power Sources*, 246 (2014) 747.
27. F.I. Dar, K.R. Moonooswamy, and M. Es-Souni, *Nano. Res. Lett*., 8 (2013) 363.
28. W. Sun, X. Rui, M. Ulaganathan, S. Madhavi, and Q. Yan, *J. Power Sources*, 295 (2015) 323.
29. H. Yan, D. Zhang, J. Xu, Y. Lu, Y. Liu, K. Qiu, Y. Zhang, and Y. Luo, *Nanoscale Res. Lett*., 9 (2014) 424.